IEEE Access
Multidisciplinary | Rapid Review | Open Access Journal

Received February 26, 2020, accepted March 5, 2020, date of publication March 9, 2020, date of current version March 20, 2020.

Digital Object Identifier 10.1109/ACCESS.2020.2979510

Integrated Factor Graph Algorithm for DOA-Based Geolocation and Tracking

MENG CHENG[1], (Member, IEEE), MUHAMMAD REZA KAHAR AZIZ[2], (Member, IEEE), AND TAD MATSUMOTO[1,3], (Fellow, IEEE)

[1]School of Information Science, Japan Advanced Institute of Science and Technology (JAIST), Nomi 923-1211, Japan
[2]Department of Electrical Engineering, Institut Teknologi Sumatera (ITERA), Lampung Selatan 35365, Indonesia
[3]Centre for Wireless Communications, University of Oulu, 90014 Oulu, Finland

Corresponding author: Meng Cheng (m-cheng@jaist.ac.jp)

This work was supported in part by the Hitachi, Ltd., and in part by the Hitachi Kokusai Electric, Inc.

ABSTRACT This paper proposes a new position tracking algorithm by integrating extended Kalman filter (EKF) and direction-of-arrival (DOA)-based geolocation into one factor graph (FG) framework. A distributed sensor network is assumed for detecting an anonymous target, where the process and observation equations in the state space model (SSM) are unknown. Importantly, the predicted state information can be utilized not only for filtering, but also for enhancing the observation process. To be specific, by taking the prediction into account as the a priori, a new FG scheme is proposed for GEolocation, denoted by FG-GE. The benefits are two-fold, compared with the conventional geolocation scheme which does not rely on the a priori information. First of all, significant performance improvement can be observed, in terms of the root mean square error (RMSE), when severe sensing errors are suddenly encountered. Furthermore, the proposed FG-GE can achieve dramatic reduction of computational complexity. In addition, this paper also proposes the use of a predicted Cramer-Rao lower bound (P-CRLB) to dynamically estimate the observation error variance, which demonstrates more robust tracking performance than that with only fixed average variance approximation.

INDEX TERMS Factor graph (FG), direction of arrival (DOA), extended Kalman filter (EKF), geolocation, tracking, complexity analysis, CRLB.

I. INTRODUCTION

The roles to be played by wireless cellular networks are experiencing a paradigm shift from mobile communications to more dedicated infrastructure-supporting applications. Emerging use cases include smart transportation, factory automation, remote construction control, intelligent agriculture [1]–[4] and etc. In particular, position-based services are gaining increased attention through the rapid evolution of cellular networks [5], [6], where tracking of the user position is believed to be of great importance. Moreover, to cope with severe attenuation of millimeter-wave (mmWave) signals in fifth generation (5G) and beyond 5G (B5G) networks [7], accurate direction identification technologies are required. For example, beam tracking is applied in massive multiple-input multiple-output (mMIMO) systems [8], [9]. Challenged by the increased density and mobility of wireless devices, low-complexity but yet highly robust geolocation and tracking techniques are strongly demanded in the future networks.

To perform tracking, an accurate geolocation scheme is required, regarded as the observation process of the state space model (SSM). Conventional geolocation schemes rely on a series of range-related measurements in time, signal strength and angle domains. For example, applications using time-of-arrival (TOA) can be found in [10], [11], where time synchronization among targets, sensors and the fusion center is assumed. Time-difference-of-arrival (TDOA) is proposed in [12], [13], which eliminates the necessity of synchronization between sensors and the target. However, it can not outperform TOA as presented in [14]. More energy efficient geolocation techniques using received-signal-strength (RSS)

The associate editor coordinating the review of this manuscript and approving it for publication was Filbert Juwono.

can be found in [15], [16]. In such cases, off-line training with reference signals has to be performed beforehand, and furthermore, the transmit signal power from the target has to be known. Due to the constraints mentioned above, time and signal strength-based schemes are not applicable if the target is anonymous. Instead, this paper proposes an efficient use of direction-of-arrival (DOA) for the following reasons: (1) neither time synchronization nor off-line training is needed; (2) DOA measurement is possible even for silent target by using camera or other sensing devices; (3) multi-path effect on DOA measurements is supposed to be negligible in future networks, due to the very densely located sensing devices, applying mmWave techniques. DOA measuring techniques are well studied such as in [17]–[19]. However, discussion of practical techniques is out of the scope of this paper.

To avoid up-link transmission congestion in distributed sensor networks, factor graph (FG) algorithm [20] is applied, where only key parameters describing the probability density function (PDF) of DOA measurements are sent from sensors to the fusion center. FG is first used for GEolocation in [21], referred to as FG-GE in this paper. It is shown to achieve higher accuracy and lower complexity than the conventional schemes. The related work can be also found in [22]–[24]. In [25], a DOA-based two-dimensional (2D) FG-GE is proposed to detect a single anonymous target, with lower root mean square error (RMSE) than the least square (LS) technique. This work has been extended to three-dimensional (3D) in [26].

In addition, a sensor separation algorithm is proposed in [26] to solve the target-DOAs matching problem in the multi-target scenario. Since messages propagated over FG-GE are all Gaussian-approximated, only the mean and the variance are needed. Therefore, the required computational complexity is very light. The first order Taylor expansion is utilized in [25] to linearize the trigonometric functions, in order to keep the Gaussianity of messages' PDF. However, such approximation still incurs a certain level of computational cost, which may get severer if the FG structure becomes large and complex.

In this paper, a new DOA-based FG-GE is proposed to further reduce the computational cost of linear approximation. Compared with the conventional approaches in [25], [26], the proposed FG-GE always utilizes predicted state information, based on the tracker output at the previous timing. In this sense, geolocation and tracking jointly work in one framework, and form an integrated FG. In order to well express the real target behavior, extended Kalman filter (EKF) is used in this paper. The complexity of conventional EKF mainly lies in matrix operations based on the linearization result with the first order Taylor series expansion. Instead, an FG-based EKF, denoted by FG-EKF, is used in this paper, as in [27]. FG-EKF replaces matrix operations by scalar operations, and therefore significantly reduces the computational complexity. Note that the complexity analysis in this paper only considers FG-GE, while the analysis of FG-EKF can be found in [27].

Besides the complexity reduction, the predicted state information is also utilized for reducing the impact of sudden sensing errors. False alarm is one of the examples, where interfering signals are also detected at the sensor in additional to the desired ones. The principle is that, the current state of target should not vary significantly from that at the previous timing. Sudden sensing errors, which may not be realized by the sensor, can be identified at the center, and then eliminated in the FG-GE detection. The prediction made by EKF can be used as the a priori information, to evaluate the measurement data. In this paper, a simple false alarm scenario is studied. It has been shown that even though the sensor may suffer from false alarm, FG-GE can still take useful measurement data from such sensor.

Known as a tuning problem, estimating the variance of observation error plays an important role in EKF, as well discussed in [28], [29]. It should be noted that in the proposed tracking system, observation is not directly modeled with Gaussian errors. Instead, target positions are detected by distributed sensors, based on a series of Gaussian-distributed DOA measurements. The smallest variance of observation error is determined by the Cramer Rao lower bound (CRLB) [30]. Due to the fact that the proposed FG-GE can achieve a performance which is very close to the CRLB, it is reasonable to use CRLB to estimate the observation error variance in real time. However, calculating CRLB requires the real target position, which is practically not available. Hence, a predicted CRLB (P-CRLB) is calculated in this paper, where the predicted target position based on the result of previous timing is used. With this technique, the proposed FG-EKF is shown to achieve higher robustness than conventional schemes which assume only fixed estimation of the observation noise variance.

The main contributions of this work are summarized as follows.

1) A new DOA-based tracking system is proposed by integrating EKF and geolocation into one FG framework;
2) By utilizing the state prediction as the a priori information, the impact of sudden sensing errors can be eliminated;
3) The proposed FG-GE exhibits much lower computational complexity than the conventional scheme;
4) The robustness of tracking is further enhanced, by estimating the observation error variance for FG-EKF with the proposed P-CRLB in real time.

The organization of this paper is as follows. The tracking model to be investigated is described in Section II. Detailed steps of the proposed FG-EKF and FG-GE algorithms are then introduced in Section III. The predicted CRLB which is utilized in FG-EKF is derived in Section IV. Moreover, the complexity analysis of FG-GE is provided in Section V. The proposed tracking system is evaluated by a series of simulations, and the results are shown in Section VI. Finally, this work is concluded with several remarks in Section VII.

II. SYSTEM MODEL

A non-linear discrete SSM is focused on in this paper. The target state at timing k is represented by $\mathbf{s}_k = [x_k, y_k]^T$, $k = \{1, 2, \ldots, K\}$, which defines the target position in a 2D plane. The process equation is given by

$$\mathbf{s}_k = f(\mathbf{s}_{k-1}) + \mathbf{w}_k, \tag{1}$$

where $f(\cdot)$ is a non-linear process function, and $\mathbf{w}_k = \left[w_{x,k}, w_{y,k}\right]^T$ represents a Gaussian-distributed noise vector, with each element following $\mathcal{N}\left(0, \sigma_w^2\right)$. According to the principle of EKF, the first order Taylor expansion is used to linearly approximate $f(\cdot)$, i.e., $f(\mathbf{s}_{k-1}) \approx f(\alpha) + f'(\alpha)(\mathbf{s}_{k-1} - \alpha)$. However, $f(\cdot)$ is unknown by the tracker, and therefore it can not be directly applied to the position tracking problem. Instead, assuming that α exists which satisfies $f(\alpha) = \mathbf{s}_{k-1}$, (1) can be rewritten by

$$\mathbf{s}_k \approx \mathbf{s}_{k-1} + \mathbf{v}_{k-1} + \mathbf{w}_k, \tag{2}$$

where the gradient $\mathbf{v}_{k-1} = f'(\alpha)(\mathbf{s}_{k-1} - \alpha)$, which can be updated during the dynamic EKF process. Note that (2) is accurate only if the target does not move very fast between any two adjacent timings.

Moreover, N distributed sensors locating at (X_n, Y_n), with $n = \{1, 2, \ldots, N\}$, are known to the fusion center. The measurement equation at sensor n and timing k can be given by

$$\hat{\theta}_{n,k} = h(n, \mathbf{s}_k) + u_{n,k}, \tag{3}$$

with $u_{n,k} \sim \mathcal{N}\left(0, \sigma_\theta^2\right)$ being the measurement noise, and $\hat{\theta}_{n,k}$ denoting the measured DOA $\theta_{n,k}$, which is the output of the non-linear measurement function $h(\cdot)$,

$$h(n, \mathbf{s}_k) = \arctan\left(\frac{Y_n - y_k}{X_n - x_k}\right). \tag{4}$$

During each sampling timing, the N sensors are assumed to obtain L snapshots of DOA, from which the PDF parameters are extracted. Let $m_{\hat{\theta}}$ and $\sigma_{\hat{\theta}}^2$ denote the mean and the variance of $\hat{\theta}$, respectively, and the indexes n and k are omitted for the simplicity. The larger the value of L, the closer the values of $m_{\hat{\theta}}$ and $\sigma_{\hat{\theta}}^2$ are to m_θ and σ_θ^2, respectively. The transmission channels between sensors and the fusion center are assumed to be error-free, and therefore no specific transmission scheme is considered in this paper.

Given the real target state, the effective observation equation can be expressed by

$$\mathbf{z}_k = g(\mathbf{s}_k) + \mathbf{e}_k, \tag{5}$$

where $\mathbf{e}_k$ denotes the observation noise vector. Since the target state is determined by the true DOAs, $g(\mathbf{s}_k)$ can be replaced by $\tilde{g}(\theta_k)$. Note that all messages in the proposed FG-GE algorithm are approximated to be Gaussian, and so is the observation noise, i.e., each element of $\mathbf{e}_k$ follows $\mathcal{N}\left(0, \sigma_e^2\right)$. However, σ_e^2 can not be directly measured. The smallest σ_e^2 which can be theoretically achieved is determined by the variances of $\hat{\theta}_k$, according to the CRLB.

III. PROPOSED TRACKING ALGORITHM

The proposed DOA-based tracking algorithm is described in this section, including both FG-EKF and FG-GE.

A. FG-EKF

According to (2) and (5), the objective of this tracking problem is to find $\mathbf{s}_k$ and $\mathbf{v}_k$ which maximize the a posterior probability $p(\mathbf{s}_k, \mathbf{v}_k | z_{1:k})$, where $(\cdot)_{1:k}$ denotes the data series from timing 1 to k. The marginal function of $\mathbf{s}_k$ and $\mathbf{v}_k$, denoted by $\hat{p}(\mathbf{s}_k, \mathbf{v}_k)$, is given by

$$\begin{aligned}\hat{p}(\mathbf{s}_k, \mathbf{v}_k) &= p(\mathbf{s}_k, \mathbf{v}_k | \mathbf{z}_{1:k}) \\ &= \sum_{\sim\mathbf{s}_k, \sim\mathbf{v}_k} p(\mathbf{s}_{1:k}, \mathbf{v}_{1:k} | \mathbf{z}_{1:k}),\end{aligned} \tag{6}$$

where $\sim$ is the exclusion operator. The conditional PDF function in (6) can be further factorized by

$$\begin{aligned}&p(\mathbf{s}_{1:k}, \mathbf{v}_{1:k} | \mathbf{z}_{1:k}) \\ &= \frac{p(\mathbf{z}_k | \mathbf{s}_{1:k}, \mathbf{v}_{1:k}, \mathbf{z}_{1:k-1})\, p(\mathbf{s}_{1:k}, \mathbf{v}_{1:k}, \mathbf{z}_{1:k-1})}{p(\mathbf{z}_{1:k})} \qquad (7) \\ &= \frac{p(\mathbf{z}_k | \mathbf{s}_k)\, p(\mathbf{s}_{1:k}, \mathbf{v}_{1:k}, \mathbf{z}_{1:k-1})}{p(\mathbf{z}_{1:k})}, \qquad (8)\end{aligned}$$

where (7) is derived based on Bayes' rule, and (8) is obtained due to that $\mathbf{z}_k$ is only determined by $\mathbf{s}_k$. Further more,

$$\begin{aligned}&\frac{p(\mathbf{s}_{1:k}, \mathbf{v}_{1:k}, \mathbf{z}_{1:k-1})}{p(\mathbf{z}_{1:k})} \\ &= \frac{p(\mathbf{s}_k | \mathbf{s}_{k-1}, \mathbf{v}_{k-1})\, p(\mathbf{v}_k | \mathbf{v}_{k-1})\, p(\mathbf{s}_{1:k-1}, \mathbf{v}_{1:k-1} | \mathbf{z}_{1:k-1})}{p(\mathbf{z}_k | \mathbf{z}_{k-1})},\end{aligned} \tag{9}$$

with the assumption that $\mathbf{s}_k$ is only determined by $\mathbf{s}_{k-1}$ and $\mathbf{v}_{k-1}$, and $\mathbf{v}_k$ is only determined by $\mathbf{v}_{k-1}$. By substituting (9) into (8), $p(\mathbf{s}_{1:k}, \mathbf{v}_{1:k} | \mathbf{z}_{1:k})$ can be re-written as

$$\begin{aligned}&p(\mathbf{s}_{1:k}, \mathbf{v}_{1:k} | \mathbf{z}_{1:k}) \\ &\propto \prod_{1:k} p(\mathbf{s}_k | \mathbf{s}_{k-1}, \mathbf{v}_{k-1})\, p(\mathbf{v}_k | \mathbf{v}_{k-1})\, p(\mathbf{z}_k | \mathbf{s}_k),\end{aligned} \tag{10}$$

where the denominator of (9), i.e. $p(\mathbf{z}_k | \mathbf{z}_{k-1})$, is ignored. Note that $p(\mathbf{s}_{1:k-1}, \mathbf{v}_{1:k-1} | \mathbf{z}_{1:k-1})$ in (9) represents the filtering result of FG-EKF at the previous timing, and therefore $\prod$ is introduced in (10) with the timing index 1 to k. Based on (10), the proposed FG-EKF algorithm can be described in the following 3 steps.

1) STATE PREDICTION

First of all, the current state prediction is performed based on the FG-EKF outputs at the previous timing. As shown in Fig. 1, the message flow of the predicted state $\mu_c(\mathbf{s}_{k|k-1})$ is given by

$$\begin{aligned}&\mu_c(\mathbf{s}_{k|k-1}) \\ &= \sum_{\mathbf{s}_{k-1}} \sum_{\mathbf{v}_{k-1}} f(\mathbf{s}_{k|k-1} | \mathbf{s}_{k-1}, \mathbf{v}_{k-1}) \mu_a(\mathbf{s}_{k-1}) \mu_b(\mathbf{v}_{k-1}),\end{aligned} \tag{11}$$

where the message flows $\mu_a(\mathbf{s}_{k-1})$ and $\mu_b(\mathbf{v}_{k-1})$ are obtained as the FG-EKF outputs at timing $k-1$, with the function $f(\mathbf{s}_{k|k-1} | \mathbf{s}_{k-1}, \mathbf{v}_{k-1}) = \mathbf{s}_{k-1} + \mathbf{v}_{k-1}$.

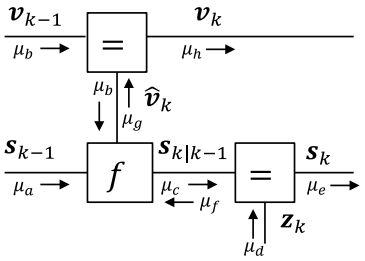

FIGURE 1. Proposed FG structure for EKF.

2) STATE REFINEMENT

Secondly, the predicted state $\mathbf{s}_{k|k-1}$ is further refined by the observation, yielding the FG-EKF results at the current timing k. As shown in Fig. 1, the message flow of the FG-EKF output $\mu_e(\mathbf{s}_k)$ is given by

$$\mu_e(\mathbf{s}_k) = \mu_c(\mathbf{s}_{k|k-1})\mu_d(\mathbf{z}_k), \tag{12}$$

where $\mu_d(\mathbf{z}_k)$ denotes the message flow of the observation, obtained by the proposed FG-GE scheme.

3) GRADIENT UPDATE

After obtaining the refined state, the vector $\mathbf{v}_k$ should also be updated. Since the process equation (1) is assumed to be unknown, $\mathbf{v}_k$ is only updated by refining $\mathbf{v}_{k-1}$ with a correction term $\hat{\mathbf{v}}_k$. According to Fig. 1, the message flow of the $\hat{\mathbf{v}}_k$ can be given by

$$\mu_g(\hat{\mathbf{v}}_k) = \sum_{\mathbf{s}_{k-1}} \sum_{\mathbf{s}_k} f(\hat{\mathbf{v}}_k|\mathbf{s}_{k-1}, \mathbf{s}_k)\mu_a(\mathbf{s}_{k-1})\mu_f(\mathbf{s}_k), \tag{13}$$

where $\mu_f(\mathbf{s}_k)$ is the message flow of the refined state, and $f(\hat{\mathbf{v}}_k|\mathbf{s}_{k-1}, \mathbf{s}_k) = \mathbf{s}_k - \mathbf{s}_{k-1}$. Finally, the message flow of the updated vector $\mathbf{v}_k$ is given by

$$\mu_h(\mathbf{v}_k) = \mu_b(\mathbf{v}_{k-1})\mu_g(\hat{\mathbf{v}}_k). \tag{14}$$

B. FG-GE

To obtain the state observation $\mathbf{z}_k$ required by FG-EKF, the proposed FG-GE is applied, which is detailed in this subsection. Note that the sensor index n is omitted in the following derivations. With the first order Taylor series expansion, the true DOA, expressed by (4), can be linearly approximated, centered at the point β, as

$$\theta_k \approx h(\beta) + \frac{\partial h(\mathbf{s}_k)}{\partial x_k}(x_k - \beta_x) + \frac{\partial h(\mathbf{s}_k)}{\partial y_k}\left(y_k - \beta_y\right), \tag{15}$$

where $\beta = [\beta_x, \beta_y]^T$. Obviously, the approximation of (15) is accurate if β is close to $\mathbf{s}_k$. In this paper, we propose that β equals to the predicted state by FG-EKF from the previous timing, i.e., $\beta = \mathbf{s}_{k|k-1}$. Therefore, (15) can be further expressed by

$$\theta_k \approx \lambda_1 x_k + \lambda_2 y_k + \lambda_3, \tag{16}$$

where λ_1, λ_2 and λ_3 are all constants, given by

$$\lambda_1 = \frac{Y - y_{k|k-1}}{(X - x_{k|k-1})^2 + (Y - y_{k|k-1})^2}, \tag{17}$$

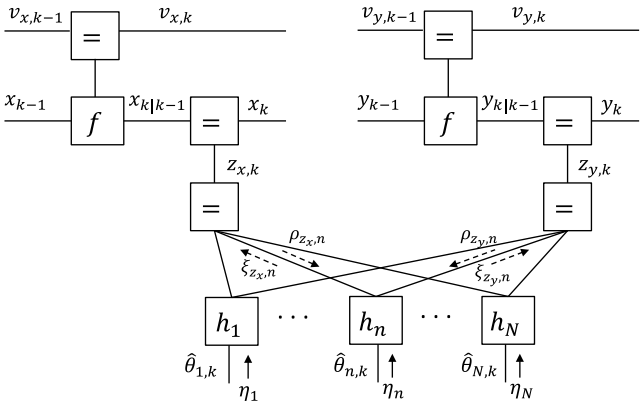

FIGURE 2. Proposed FG detector for the DOA-based geolocation.

$$\lambda_2 = \frac{-(X - x_{k|k-1})}{(X - x_{k|k-1})^2 + (Y - y_{k|k-1})^2}, \tag{18}$$

$$\lambda_3 = \frac{-(Y - y_{k|k-1})x_{k|k-1} + (X - x_{k|k-1})y_{k|k-1}}{(X - x_{k|k-1})^2 + (Y - y_{k|k-1})^2} + \arctan\left(\frac{Y - y_{k|k-1}}{X - x_{k|k-1}}\right). \tag{19}$$

Therefore, the target position can be linearly expressed by

$$x_k = \frac{\theta_k - \lambda_2 y_k - \lambda_3}{\lambda_1}, \tag{20}$$

$$y_k = \frac{\theta_k - \lambda_1 x_k - \lambda_3}{\lambda_2}. \tag{21}$$

Given the Gaussian-distributed DOA measurements as the input of FG-GE, all messages interchanged inside FG-GE are also Gaussian, where linear approximations at the function nodes follow (20) and (21).

The proposed FG-GE structure is illustrated in Fig. 2, as a part of the integrated tracking system. Let η_n denote the message flow of the measured DOA associated with the function node h_n. In the upward process, $\xi_{z_x,n}$ and $\xi_{z_y,n}$ denote the messages forwarded from h_n to z_x and z_y, respectively. Then, $\rho_{z_x,n}$ and $\rho_{z_y,n}$ are the downward messages arriving at h_n from z_x and z_y, respectively. The detailed updates at the function node h_n can be described by two steps as follows.

1) Update of $\xi_{z_x,n}$:

$$m_{\xi_{z_x,n}} = \frac{1}{\lambda_{n,1}} m_{\eta_k} - \frac{\lambda_{n,2}}{\lambda_{n,1}} m_{\rho_{z_y,n}} - \frac{\lambda_{n,3}}{\lambda_{n,1}}, \tag{22}$$

$$\sigma^2_{\xi_{z_x,n}} = \frac{1}{\lambda^2_{n,1}}\sigma^2_{\eta_n} + \left(\frac{\lambda_{n,2}}{\lambda_{n,1}}\right)^2 \sigma^2_{\rho_{z_y,n}}, \tag{23}$$

$$m_{\xi_{z_y,n}} = \frac{1}{\lambda_{n,2}} m_{\eta_k} - \frac{\lambda_{n,1}}{\lambda_{n,2}} m_{\rho_{z_x,n}} - \frac{\lambda_{n,3}}{\lambda_{n,2}}, \tag{24}$$

$$\sigma^2_{\xi_{z_y,n}} = \frac{1}{\lambda^2_{n,2}}\sigma^2_{\eta_n} + \left(\frac{\lambda_{n,1}}{\lambda_{n,2}}\right)^2 \sigma^2_{\rho_{z_x,n}}, \tag{25}$$

2) Update of $\rho_{z_x,n}$:

$$\sigma^2_{\rho_{z_x,n}} = \frac{1}{\sum_{i\in\{1:N\}, i\neq n} \sigma^2_{\xi_{z_x,i}}}, \tag{26}$$

$$m_{\rho_{z_x,n}} = \sigma^2_{\rho_{z_x,n}} \sum_{i\in\{1:N\},i\neq n} \frac{m_{\xi_{z_x,i}}}{\sigma^2_{\xi_{z_x,i}}}, \tag{27}$$

$$\sigma^2_{\rho_{z_y,n}} = \frac{1}{\sum_{i\in\{1:N\},i\neq n} \sigma^2_{\xi_{z_y,i}}}, \tag{28}$$

$$m_{\rho_{z_y,n}} = \sigma^2_{\rho_{z_y,n}} \sum_{i\in\{1:N\},i\neq n} \frac{m_{\xi_{z_y,i}}}{\sigma^2_{\xi_{z_y,i}}}. \tag{29}$$

The iteration is to be performed at the function node 1 to N, with the estimated position $m_{\mathbf{z}} = \left[m_{z_x}, m_{z_y}\right]^T$ obtained by

$$m_{z_x} = \sigma^2_{z_x} \sum_{i\in\{1:N\}} \frac{m_{\xi_{z_x,i}}}{\sigma^2_{\xi_{z_x,i}}}, \tag{30}$$

$$m_{z_y} = \sigma^2_{z_y} \sum_{i\in\{1:N\}} \frac{m_{\xi_{z_y,i}}}{\sigma^2_{\xi_{z_y,i}}}, \tag{31}$$

and

$$\sigma^2_{z_x} = \frac{1}{\sum_{i\in\{1:N\}} \sigma^2_{\xi_{z_x,i}}}, \tag{32}$$

$$\sigma^2_{z_y} = \frac{1}{\sum_{i\in\{1:N\}} \sigma^2_{\xi_{z_y,i}}}. \tag{33}$$

It should be noted that $\sigma^2_{\mathbf{z}} = \left[\sigma^2_{z_x}, \sigma^2_{z_y}\right]^T$ denotes the variance vector of the FG-GE estimation. However, according to the observation equation defined in (5), $g(\mathbf{s}_k)$ is a constant, and therefore the observation variance of $\mathbf{z}_k$ is equal to σ^2_e, which is different from the results in (32) and (33). The observation variance is calculated in the following section.

IV. P-CRLB DERIVATION

In this section, a P-CRLB is derived for the proposed EKF, as the estimate of the observation noise variance. First of all, by omitting the timing index k, the CRLB is given by [25]

$$\text{CRLB} = \text{trace}\left[F^{-1}(\mathbf{s})\right], \tag{34}$$

where F denotes the Fisher information matrix (FIM). Given the measured DOA variable $\hat{\theta}$ with L samples, the FIM can be expressed by

$$F(\mathbf{s}) = E\left[\left(\frac{\partial}{\partial \mathbf{s}} \ln p\left(\hat{\theta}\right)\right)^2\right], \tag{35}$$

where the Gaussian PDF function of $\hat{\theta}$ is given by

$$p(\hat{\theta}) = \prod_{l=1}^{L} \frac{1}{\sqrt{2\pi\sigma^2_\theta}} \exp\left[-\frac{1}{2\sigma^2_\theta}\left(\hat{\theta}_l - \theta\right)^2\right]. \tag{36}$$

Moreover, due to the fact that

$$E\left[\left(\frac{\partial}{\partial \theta} \ln p(\hat{\theta})\right)^2\right] = -E\left[\frac{\partial^2}{\partial \theta^2} \ln p(\hat{\theta})\right], \tag{37}$$

and according to (36),

$$\frac{\partial^2}{\partial \theta^2} \ln p(\hat{\theta}) = -\frac{L}{\sigma^2_\theta}. \tag{38}$$

Then, the FIM can further be derived by

$$\begin{aligned} F(\mathbf{s}) &= \frac{\partial \theta}{\partial \mathbf{s}}^T E\left[\left(\frac{\partial}{\partial \theta} \ln p(\hat{\theta})\right)^T \left(\frac{\partial}{\partial \theta} \ln p(\hat{\theta})\right)\right] \frac{\partial \theta}{\partial \mathbf{s}} \\ &= \frac{\partial \theta}{\partial \mathbf{s}}^T E\left[\left(\frac{\partial}{\partial \theta} \ln p(\hat{\theta})\right)^2\right] \frac{\partial \theta}{\partial \mathbf{s}} \\ &= \frac{\partial \theta}{\partial \mathbf{s}}^T \left[\frac{L}{\sigma^2_\theta}\right] \frac{\partial \theta}{\partial \mathbf{s}}, \end{aligned} \tag{39}$$

where $\frac{\partial \theta}{\partial \mathbf{s}}$ is defined by the Jacobian matrix,

$$\mathbf{J} = \frac{\partial \theta}{\partial \mathbf{s}} = \begin{bmatrix} \frac{\partial \theta_1}{\partial x} & \frac{\partial \theta_1}{\partial y} \\ \frac{\partial \theta_2}{\partial x} & \frac{\partial \theta_2}{\partial y} \\ \vdots & \vdots \\ \frac{\partial \theta_N}{\partial x} & \frac{\partial \theta_N}{\partial y} \end{bmatrix}, \tag{40}$$

with

$$\frac{\partial \theta_n}{\partial x} = \frac{Y_n - y}{d_n^2}, \tag{41}$$

$$\frac{\partial \theta_n}{\partial y} = \frac{-(X_n - x)}{d_n^2}, \tag{42}$$

and the Euclidean distance between sensor n and the target in the 2D plane is denoted by d_n, with $n = \{1, 2, \ldots, N\}$. Finally, the CRLB of the proposed geolocation system can be expressed by

$$\text{CRLB} = \left\{\text{trace}\left[\left(\mathbf{J}^T \Sigma_\theta^{-1} \mathbf{J}\right) L\right]\right\}^{-1}. \tag{43}$$

However, since the real target position is unknown in practice at the timing k, x_k and y_k in (41) and (42) are replaced by $x_{k|k-1}$ and $y_{k|k-1}$, respectively, with which (40) can be rewritten as

$$\mathbf{J_{k|k-1}} = \begin{bmatrix} \frac{Y_1 - y_{k|k-1}}{d_1^2} & \frac{-(X_1 - x_{k|k-1})}{d_1^2} \\ \frac{Y_2 - y_{k|k-1}}{d_2^2} & \frac{-(X_2 - x_{k|k-1})}{d_2^2} \\ \vdots & \vdots \\ \frac{Y_N - y_{k|k-1}}{d_N^2} & \frac{-(X_N - x_{k|k-1})}{d_N^2} \end{bmatrix}. \tag{44}$$

Finally, the P-CRLB can be obtained as

$$\text{P-CRLB} = \left\{\text{diag}\left[\left(\mathbf{J}_{k|k-1}^T \Sigma_\theta^{-1} \mathbf{J}_{k|k-1}\right) L\right]\right\}^{-1}. \tag{45}$$

V. COMPLEXITY COMPARISON

The complexity comparison between the proposed FG-GE and the conventional FG-GE in [25] is provided in this section. Specifically, the required addition (ADD), multiplication (MUL) and trigonometric (TRI) operations for the both schemes within one iteration time are listed in Tables 1-2.

TABLE 1. Arithmetic complexity analyses of the proposed FG-GE.

Proposed FG-GE algorithm		
Step	Calculation	Operation
Constant terms related to λ_1, λ_2 and λ_3 in (22)-(25)	$\frac{1}{\lambda_1}, \frac{1}{\lambda_2}, \frac{1}{\lambda_1^2}, \frac{1}{\lambda_2^2}, \frac{\lambda_3}{\lambda_1}, \frac{\lambda_3}{\lambda_2}, \left(\frac{\lambda_2}{\lambda_1}\right)^2, \left(\frac{\lambda_1}{\lambda_2}\right)^2, \arctan\left(\frac{Y-y_{k\|k-1}}{X-x_{k\|k-1}}\right)$ based on (17)-(19)	5 ADD 10 MUL 1 TRI
$m_{\xi_{z_x}}$ and $\sigma^2_{\xi_{z_x}}$	(22) and (23), assuming the constant terms are given	$3J$ ADD $4J$ MUL 0 TRI
$m_{\xi_{z_y}}$ and $\sigma^2_{\xi_{z_y}}$	(24) and (25), assuming the constant terms are given	$3J$ ADD $4J$ MUL 0 TRI
Total		5+6J ADD 10+8J MUL 1 TRI

TABLE 2. Arithmetic complexity analyses of the conventional FG-GE.

Conventional FG-GE algorithm		
Step	Calculation	Operation
$\mu_{F\mapsto\Delta y}$	$m_{\Delta x}\tan(m_{\hat{\theta}})$, $\sigma^2_{\Delta x}\tan^2(m_{\hat{\theta}}) + m^2_{\Delta x}\sigma^2_{\hat{\theta}}\sec^4(m_{\hat{\theta}})$ $+\sigma^2_{\Delta x}\sigma^2_{\hat{\theta}}\sec^4(m_{\hat{\theta}})$	$2J$ ADD $10J$ MUL $2J$ TRI
$\mu_{F\mapsto\Delta x}$	$m_{\Delta y}\tan(m_{\hat{\theta}})$, $\sigma^2_{\Delta y}\tan^2(m_{\hat{\theta}}) + m^2_{\Delta y}\sigma^2_{\hat{\theta}}\sec^4(m_{\hat{\theta}})$ $+\sigma^2_{\Delta y}\sigma^2_{\hat{\theta}}\sec^4(m_{\hat{\theta}})$	$2J$ ADD $10J$ MUL $2J$ TRI
$x \leftrightarrow \Delta x$ $y \leftrightarrow \Delta y$	$m_{\Delta x} = X - m_x$ $m_{\Delta y} = X - m_y$ $m_x = X - m_{\Delta x}$ $m_y = X - m_{\Delta y}$	$4J$ ADD 0 MUL 0 TRI
Total		$8J$ ADD $20J$ MUL $4J$ TRI

Note that we assume subtraction and division have the same complexity as addition and multiplication, respectively, for the sake of simplicity. Moreover, only the upward message flows as shown in Fig. 2 are considered, while the downward messages from the variable nodes z_x and z_y to the function nodes are not included, since they are identical for the two schemes compared.

As shown in Table 1, λ_1, λ_2 and λ_3 are all constants during the proposed FG-GE detection at each timing, and the required operations do not increase proportionally to the iteration time J. Moreover, only one trigonometric operation is needed in the proposed FG-GE. However, the complexities of the conventional FG-GE are found to be completely proportional to J, as shown in Table 2. In addition, more trigonometric operations are included as J increases. Therefore, our proposed FG-GE scheme is found less complicated compared to the conventional one.

VI. SIMULATIONS

In this section, an illustrative non-linear SSM is evaluated with the proposed tracking algorithm. With the timing

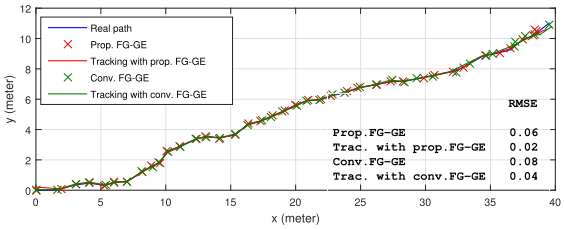

(a) Scenario : indoor.

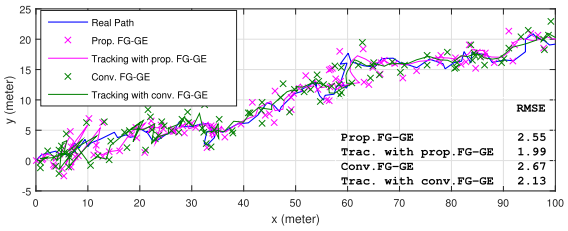

(b) Scenario 2: outdoor.

FIGURE 3. Performance comparison between the proposed and conventional schemes.

$k = \{1, 2, \ldots, 100\}$, the process equations are given by

$$x_k = x_{k-1} + \cos\left(\frac{x_{k-1}\phi}{k}\right) + w_{x,k}, \tag{46}$$

$$y_k = y_{k-1} + \sin\left(\frac{y_{k-1}\phi}{k}\right) + w_{y,k}, \tag{47}$$

where ϕ is set at $\pi/60$. The initial state $\mathbf{s}_0 = [x_0, y_0]^T = [0, 0]^T$. Simulations aiming at different investigation purposes are presented as follows.

A. FG-GE COMPARISON

In this sub-section, comparison between the proposed and the conventional counterpart schemes is provided under two scenarios. In Scenario 1, an indoor environment is considered, where three distributed sensors are deployed at (0,-1), (8,10) and (15, -2), respectively, with the unit being meter. At each timing, every sensor is assumed to measure 60 DOA samples, i.e., $L = 60$. $\sigma_w^2 = 0.05$ and $\sigma_\theta^2 = 3°$ were also assumed. Scenario 2 focuses on the outdoor environment, with three sensors located at (0,-10), (80,100) and (150, -20), respectively, and the measurement snapshot number $L = 70$. Moreover, $\sigma_w^2 = 1$ and $\sigma_\theta^2 = 5°$ were set. For fair comparison, the FG iteration time $J = 10$ was fixed, and the same random seed was used. Note that the conventional FG-GE applied in the simulation follows [25].

The detected target positions using FG-GE, as well as the tracking results are shown in Fig. 3. Clearly, in the both scenarios, the proposed FG-GE can achieve slightly lower root mean square errors (RMSEs) than that with the conventional scheme. The improvement is not significant because in such a stable sensing environment, even with the conventional scheme, close-CRLB performance can be achieved, and hence the room for further improvement is limited. The same performance trends can be observed when testing other random seeds in the simulation, but the results are omitted

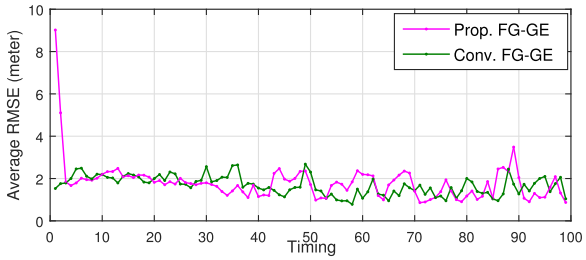

(a) $\hat{\mathbf{s}}_{1|0} = [10, 15]^T$ in the proposed FG-GE.

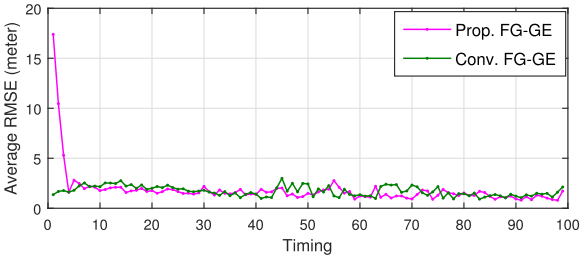

(b) $\hat{\mathbf{s}}_{1|0} = [15, 20]^T$ in the proposed FG-GE.

FIGURE 4. Convergence analysis of the tracking timing index.

due to the space limitation. Note that the proposed scheme can achieve centimeter level RMSEs in indoor scenario, as shown in Fig. 3(a), which is supposed to satisfy the geolocation requirment in 6G systems [31].

Note that with the conventional FG-GE, the detection performances do not vary significantly at different timings. However, with the proposed FG-GE, a prediction of the current state is always needed. Therefore, large errors may happen at the initial stage, due to the lack of initial state prediction. In this sub-section, the impact of the initialization is neglected by assuming that the initial state prediction is known by the tracker. More detailed discussions are provided in the next sub-section.

B. CONVERGENCE

Due to the difficulty of theoretical analyses, the convergence behavior of the proposed FG-GE is investigated only by simulations in this sub-section. Specifically, it was evaluated in terms of two parameters, i.e., the timing index and the FG iterations.

First of all, the convergence behavior versus timing index is evaluated. In order to compare the average RMSE, 100 simulations were performed for the proposed and the conventional FG-GE schemes at each timing. The other parameters were set the same as in Scenario 2 defined in the previous sub-section. Note that for the proposed FG-GE, prediction of the first state $\hat{\mathbf{s}}_{1|0}$ was randomly chosen. In the first simulation, $\hat{\mathbf{s}}_{1|0} = [10, 15]^T$ was used. It can be clearly seen from Fig. 4(a) that the average RMSE of the proposed FG-GE is around 9 meters at $k = 1$, compared to 1.8 meters with the conventional scheme. However, it quickly converges to almost the same level as that of the conventional scheme after the 3rd timing.

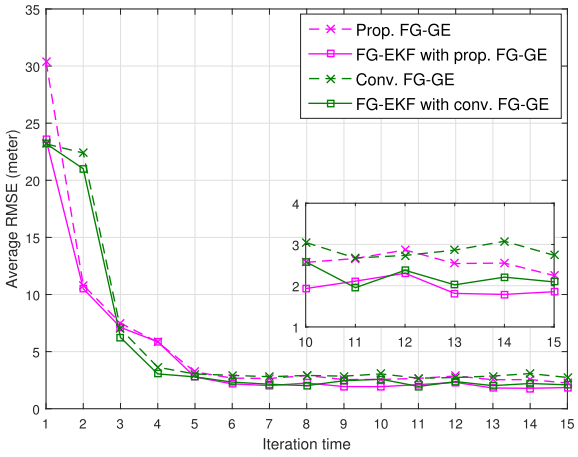

FIGURE 5. Convergence analysis of the FG iteration time.

According to Fig. 4(b), with $\hat{\mathbf{s}}_{1|0} = [15, 25]^T$, the average RMSE with the proposed FG-GE is 17.5 meters at $k = 1$, which is larger than the previous case, because $\hat{\mathbf{s}}_{1|0}$ is farther from the real target position. It is found that, the initial RMSE of the proposed FG-GE depends on the state prediction at $k = 1$, but quickly converges after only 3 to 4 rounds of computations. Therefore, the initial convergence problem of the proposed FG-GE can be negligible in the tracking phase.

Then, the convergence behavior was evaluated versus the FG iterations. As mentioned in Section V, the proposed FG-GE requires less computations than that of the conventional scheme for each FG iteration. However, the real system complexity should also consider the FG iteration time required to achieve the performance convergence. Specifically, the average RMSEs of the two schemes are simulated versus J. The other parameters were set the same as that defined in Scenario 2 of Section VI-A.

According to Fig. 5, after the first round of FG iteration, the proposed FG-GE achieves an average RMSE at 30.5 meters, which is roughly 6 meters larger than that of the conventional scheme. However, the average RMSEs of the both schemes quickly converge after around 5 to 6 iterations. This observation clearly indicates that the proposed FG-GE does not require more FG iterations compared with the conventional scheme.

C. FALSE ALARM

In this sub-section, the robustness of the proposed FG-GE is presented when the DOA measurement suffers from false alarm. A simple scenario is evaluated in this simulation, i.e., false alarm happens at each timing with a probability p_f for only one of the deployed sensors. If it happens, interfering signals with random DOAs will be observed at the sensor, besides the measurement of the real target. With the conventional FG-GE, the measurement data from the sensor in false alarm will not be used for detection at the fusion center, because separating the real and the interfering DOA measurements is difficult. However, with our proposed FG-GE scheme, false alarm signals can be identified, if measured

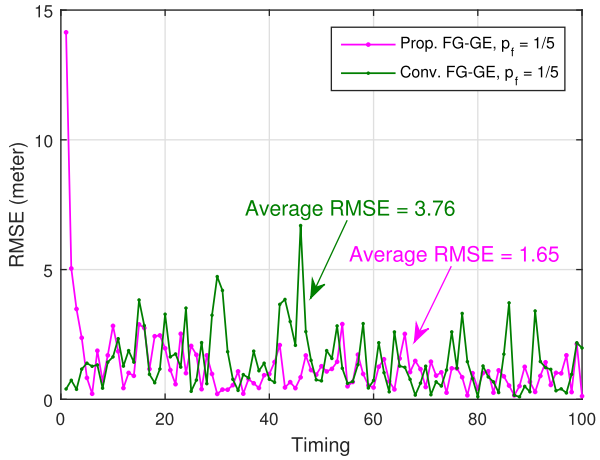

FIGURE 6. Performance evaluation of FG-GE with false alarm.

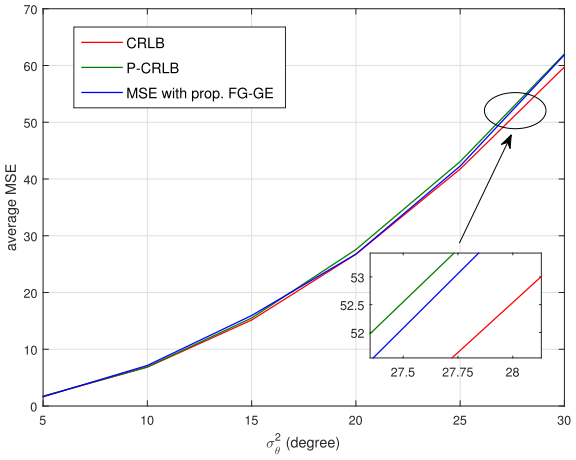

FIGURE 7. Performance comparison among P-CRLB, real CRLB and the average MSE with the proposed FG-GE.

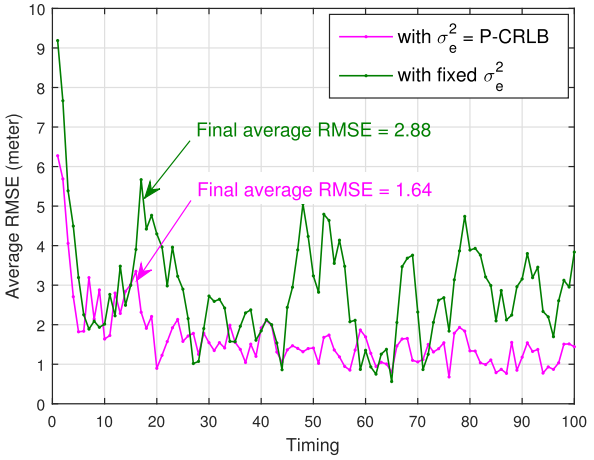

FIGURE 8. Average RMSE evaluation with different strategies of observation noise variances.

DOAs are outside of the degree range threshold. The degree range threshold was set at $\pm 20°$, compared with the predicted DOA based on the a priori information, and $p_f = 1/5$. The rest of parameters followed the Scenario 2 of Section VI-A.

As shown in Fig. 6, the proposed FG-GE is more stable, with the average RMSE equal to 1.65 meters. However, the conventional scheme exhibits larger estimation variances caused by false alarm, with the average RMSE twice as large as that of the proposed scheme. Therefore, utilizing the a priori information at the FG-GE is proved to achieve higher stability, because the more the useful DOA measurements, the better the detection performance. Note that the average RMSE is calculated only considering the performances with the timing $k > 5$, in order to eliminate the influence of the initial convergence behavior.

D. P-CRLB

The utilization of P-CRLB is motivated by the fact that, the observation stability, expressed by the variance σ_e^2, may dynamically change in practical tracking environments. To keep the tracking performance stable, P-CRLB is used as the estimate of σ_e^2 in real time. The estimation accuracy is evaluated by comparing three items, i.e., the P-CRLB, the real CRLB and the average mean square error (MSE) achieved by the proposed FG-GE. The average MSE mentioned above is equivalent to the average σ_e^2. Note that σ_e^2 is practically determined by the measurement variance σ_θ^2, which is always kept the same for all sensors in order to observe the global effect trend. The other parameters are set the same as those defined in Scenario 2 of Section VI-A.

First of all, it is found from Fig. 7 that the gap of average MSE curves between the proposed FG-GE and the real CRLB is very minor, especially when σ_θ^2 values are small. This observation implies an excellent geolocation performance of the proposed FG-GE. Moreover, the P-CRLB curve is found to be very close to that of the average MSE achieved by the simulations. Therefore, estimating the observation noise variance by P-CRLB is proved to be very accurate.

To further evaluate the robustness of FG-EKF using P-CRLB, simulations were conducted with dynamic DOA measurement variances. Specifically, at each timing, σ_θ^2 was randomly chosen from the set $\{2°, 6°, 10°, 14°, 18°\}$, but still kept the same for all sensors. With the proposed technique, P-CRLB was dynamically calculated as the estimate of σ_e^2, required in the FG-EKF calculation. However, in the comparative scheme, only fixed σ_e^2 is used, assuming that the observation error statistics can be obtained through the offline tests. In fact, evaluating the proposed FG-GE independently of FG-EKF is not feasible, as described in Section IV. Therefore, in this simulation, only approximated average σ_e^2 was used, which was calculated as the MSE with the proposed FG-GE.

As shown in Fig. 8, the average RMSEs with dynamic P-CRLB are in general lower than that with the fixed σ_e^2. After further averaging the RMSEs over all timings, the final average RMSE achieved by the proposed technique is 1.64 meters, which is 1.24 meters smaller than that with the conventional scheme compared. Therefore, the proposed FG-EKF using P-CRLB exhibits higher robustness against dynamic environment changes than that with the case of offline average error estimation.

VII. CONCLUSION

This paper has proposed a DOA-based tracking algorithm, which integrates EKF and geolocation into one FG framework. The predicted state information obtained from EKF is used not only for filtering, but also for observation, i.e, as the a priori information of FG-GE. According to the simulation results, the proposed FG-GE can always achieve lower average RMSEs than that with conventional schemes. Although large errors may happen at the beginning of tracking due to the lack of accurate a priori, it has been shown that the detection performance quickly converges after only 3 or 4 timings. Moreover, the impact of sudden sensing errors, such as false alarm, can be effectively reduced by utilizing the a priori information. In addition, the P-CRLB is used in FG-EKF to estimate the variance of observation error. With this technique, tracking is made more robust in the presence of dynamic environment change, compared with the scheme using fixed estimation of the observation variance. The proposed tracking system can be easily implemented in practice due to its low complexity.

REFERENCES

[1] B. Holfeld, D. Wieruch, T. Wirth, L. Thiele, S. A. Ashraf, J. Huschke, I. Aktas, and J. Ansari, "Wireless communication for factory automation: An opportunity for LTE and 5G systems," *IEEE Commun. Mag.*, vol. 54, no. 6, pp. 36–43, Jun. 2016.

[2] N.-S. Vo, T. Q. Duong, M. Guizani, and A. Kortun, "5G optimized caching and downlink resource sharing for smart cities," *IEEE Access*, vol. 6, pp. 31457–31468, 2018.

[3] S. A. A. Shah, E. Ahmed, M. Imran, and S. Zeadally, "5G for vehicular communications," *IEEE Commun. Mag.*, vol. 56, no. 1, pp. 111–117, Jan. 2018.

[4] R. Li, Z. Zhao, X. Zhou, G. Ding, Y. Chen, Z. Wang, and H. Zhang, "Intelligent 5G: When cellular networks meet artificial intelligence," *IEEE Wireless Commun.*, vol. 24, no. 5, pp. 175–183, Oct. 2017.

[5] H. Wymeersch, G. Seco-Granados, G. Destino, D. Dardari, and F. Tufvesson, "5G mmWave positioning for vehicular networks," *IEEE Wireless Commun.*, vol. 24, no. 6, pp. 80–86, Dec. 2017.

[6] M. Koivisto, A. Hakkarainen, M. Costa, P. Kela, K. Leppanen, and M. Valkama, "High-efficiency device positioning and location-aware communications in dense 5G networks," *IEEE Commun. Mag.*, vol. 55, no. 8, pp. 188–195, Aug. 2017.

[7] A. Ghosh, A. Maeder, M. Baker, and D. Chandramouli, "5G evolution: A view on 5G cellular technology beyond 3GPP release 15," *IEEE Access*, vol. 7, pp. 127639–127651, 2019.

[8] F. Liu, P. Zhao, and Z. Wang, "EKF-based beam tracking for mmWave MIMO systems," *IEEE Commun. Lett.*, vol. 23, no. 12, pp. 2390–2393, Dec. 2019.

[9] J. Zhao, F. Gao, W. Jia, S. Zhang, S. Jin, and H. Lin, "Angle domain hybrid precoding and channel tracking for millimeter wave massive MIMO systems," *IEEE Trans. Wireless Commun.*, vol. 16, no. 10, pp. 6868–6880, Oct. 2017.

[10] M. Khalaf-Allah, "Time of arrival (TOA)-based direct location method," in *Proc. 16th Int. Radar Symp. (IRS)*, Jun. 2015, pp. 812–815.

[11] T. Qiao and H. Liu, "An improved method of moments estimator for TOA based localization," *IEEE Commun. Lett.*, vol. 17, no. 7, pp. 1321–1324, Jul. 2013.

[12] H. Ni, G. Ren, and Y. Chang, "A TDOA location scheme in OFDM based WMANs," *IEEE Trans. Consum. Electron.*, vol. 54, no. 3, pp. 1017–1021, Aug. 2008.

[13] L. Yang, J. Cao, and W. Yang, "TDOA location based on modified Newton method," in *Proc. IEEE 13th Int. Conf. Signal Process. (ICSP)*, Nov. 2016, pp. 1515–1518.

[14] T. Qiao, S. Redfield, A. Abbasi, Z. Su, and H. Liu, "Robust coarse position estimation for TDOA localization," *IEEE Wireless Commun. Lett.*, vol. 2, no. 6, pp. 623–626, Dec. 2013.

[15] C.-T. Huang, C.-H. Wu, Y.-N. Lee, and J.-T. Chen, "A novel indoor RSS-based position location algorithm using factor graphs," *IEEE Trans. Wireless Commun.*, vol. 8, no. 6, pp. 3050–3058, Jun. 2009.

[16] H. Laitinen, S. Juurakko, T. Lahti, R. Korhonen, and J. Lahteenmaki, "Experimental evaluation of location methods based on signal-strength measurements," *IEEE Trans. Veh. Technol.*, vol. 56, no. 1, pp. 287–296, Jan. 2007.

[17] S. Gong, H. Xiong, M. Peng, X. Ding, and H. Tang, "Joint DOD and DOA estimation for bistatic multiple-input multiple-output radar target discrimination based on improved unitary ESPRIT method," *IET Commun.*, vol. 12, no. 12, pp. 1397–1405, Jul. 2018.

[18] Q. Xie, X. Pan, M. Huang, J. Chen, and S. Xiao, "Sparsity-based direction-of-departure and direction-of-arrival estimation for bistatic multiple-input multiple-output radar," *IEEE Access*, vol. 7, pp. 118826–118838, 2019.

[19] Q. Xie, X. Pan, J. Chen, and S. Xiao, "Joint DOD and DOA estimation for coherently distributed sources in bistatic MIMO radar based on joint diagonalization," *IEEE Access*, vol. 7, pp. 107805–107815, 2019.

[20] H.-A. Loeliger, J. Dauwels, J. Hu, S. Korl, L. Ping, and F. R. Kschischang, "The factor graph approach to model-based signal processing," *Proc. IEEE*, vol. 95, no. 6, pp. 1295–1322, Jun. 2007.

[21] J.-C. Chen, C.-S. Maa, and J.-T. Chen, "Factor graphs for mobile position location," in *Proc. IEEE Int. Conf. Acoust., Speech, Signal Process. (ICASSP)*, vol. 2, Apr. 2003, pp. 393–396.

[22] C.-T. Huang, C.-H. Wu, Y.-N. Lee, and J.-T. Chen, "A novel indoor RSS-based position location algorithm using factor graphs," *IEEE Trans. Wireless Commun.*, vol. 8, no. 6, pp. 3050–3058, Jun. 2009.

[23] C. Mensing and S. Plass, "TDOA positioning based on factor graphs," in *Proc. IEEE 17th Int. Symp. Pers., Indoor Mobile Radio Commun.*, Sep. 2006, pp. 1–5.

[24] J.-C. Chen, Y.-C. Wang, C.-S. Maa, and J.-T. Chen, "Network-side mobile position location using factor graphs," *IEEE Trans. Wireless Commun.*, vol. 5, no. 10, pp. 2696–2704, Oct. 2006.

[25] M. R. Kahar Aziz, K. Anwar, and T. Matsumoto, "A new DOA-based factor graph geolocation technique for detection of unknown radio wave emitter position using the first-order Taylor series approximation," *EURASIP J. Wireless Commun. Netw.*, vol. 2016, no. 1, p. 189, Dec. 2016.

[26] M. Cheng, M. R. K. Aziz, and T. Matsumoto, "A DOA-based factor graph technique for 3D multi-target geolocation," *IEEE Access*, vol. 7, pp. 94630–94641, 2019.

[27] H.-L. Jhi, J.-C. Chen, C.-H. Lin, and C.-T. Huang, "A factor-graph-based TOA location estimator," *IEEE Trans. Wireless Commun.*, vol. 11, no. 5, pp. 1764–1773, May 2012.

[28] R. Zanetti, "Recursive update filtering for nonlinear estimation," *IEEE Trans. Autom. Control*, vol. 57, no. 6, pp. 1481–1490, Jun. 2012.

[29] M. Saha, R. Ghosh, and B. Goswami, "Robustness and sensitivity metrics for tuning the extended Kalman filter," *IEEE Trans. Instrum. Meas.*, vol. 63, no. 4, pp. 964–971, Apr. 2014.

[30] Z. Lin, Q. Zou, E. S. Ward, and R. J. Ober, "Cramer-rao lower bound for parameter estimation in nonlinear systems," *IEEE Signal Process. Lett.*, vol. 12, no. 12, pp. 855–858, Dec. 2005.

[31] M. Latva-Aho and K. Leppänen, "Key driver and research challenges for 6G ubiquitous wireless intelligence, version 1," Univ. Oulu, Oulu, Finland, White Paper, Sep. 2019.

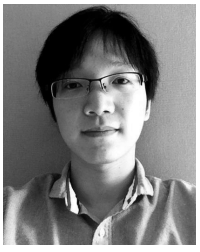

MENG CHENG (Member, IEEE) received the B.Eng. degree in telecommunication engineering from the Anhui University of Technology, Anhui, China, in 2009, the M.Sc. degree (Hons.) in wireless communications from the University of Southampton, Southampton, U.K., in 2010, and the Ph.D. degree in information science from the Japan Advanced Institute of Science and Technology (JAIST), Ishikawa, Japan, in 2014. He served as a 5G Research Engineer with the Shanghai Research Center, Huawei Technologies Company, Ltd., from 2014 to 2017. After that, he returned to JAIST as a Postdoctoral Researcher. His research interests are network information theory, non-orthogonal multiple access (NOMA), iterative coding/decoding, and wireless geolocation techniques.

MUHAMMAD REZA KAHAR AZIZ (Member, IEEE) was born in Bandar Lampung, Indonesia, in 1981. He received the bachelor's and master's degrees *(cum laude)* in electrical engineering (telecommunications) from the Institut Teknologi Bandung (ITB), Bandung, Indonesia, in 2004 and 2012, respectively, and the Ph.D. degree in information science from the Japan Advanced Institute of Science and Technology (JAIST), Ishikawa, Japan, in 2016. In 2005, he has joined the MERCATOR Summer School, University of Duisburg Essen (UDE), Universitas Indonesia (UI) Campus, Jakarta, Indonesia. From 2004 to 2005, he was a Microwave Radio Service Engineer and a Project Coordianator in Siemens Indonesia. Then, he had been with Ericsson Indonesia (EID) as a Broadband Solution Engineer for Wireless and Optical Transport from 2005 to 2010, where he was also selected as Ericsson Microwave Radio Champion for Indonesia region. In 2011, he served as a Teaching Assistant with ITB and an Adjunct Lecturer with Institut Teknologi Telkom (ITT). Since 2012, he has been with the Institut Teknologi Sumatera (ITERA), Lampung, Indonesia, as a Teaching Staff. He also received Graduate Research Program (GRP) and a Doctor Research Fellow (DRF) from JAIST, from 2013 to 2016. In February 2020, he received the IEEE Journal Award by the IEEE Indonesia Section. His research interests include wireless communication systems, signal processing, information theory, radio geolocation, factor graph, antennas, and electromagnetic.

Dr. Reza received award of 10% top performer Ericsson Indonesia employee in 2009 and ITB Voucher Scholarship in 2011. He received Best Paper Award in 9th Asia Modeling Symposium (AMS) 2015, Kuala Lumpur, Malaysia, and the 2nd Symposium of Future Telecommunication and Technologies (SOFTT) 2018, Bandung, Indonesia. JAIST Foundation Research Grant for Students was obtained for attending the European Wireless Conference 2016, Oulu, Finland. He also received research grant of Hibah Mandiri from ITERA, in 2017. He is currently serving as a Reviewer and TPC for IEEE conferences, e.g., ICC, GLOBECOM, VTC, and others, and several journals including IEEE TVT and Access.

TAD MATSUMOTO (Fellow, IEEE) received the B.S. and M.S. degrees in electrical engineering under the mentorship of Prof. S.-I. Takahashi, and the Ph.D. degree in electrical engineering under the supervision of Prof. M. Nakagawa from Keio University, Yokohama, Japan, in 1978, 1980, and 1991, respectively.

In 1980, he joined Nippon Telegraph and Telephone Corporation (NTT), where he was involved in a lot of research and development projects, all for mobile wireless communications systems. In 1992, he transferred to NTT DoCoMo, where he researched on code-division multiple-access techniques for mobile communication systems. In 1994, he transferred to NTT America, where he served as a Senior Technical Advisor of a joint project between NTT and NEXTEL Communications. From 1996 to 2001, he returned to NTT DoCoMo, where he served as the Head of the Radio Signal Processing Laboratory. He researched on adaptive signal processing, multiple-input multiple-output turbo signal detection, interference cancellation, and space-time coding techniques for broadband mobile communications. In 2002, he moved to the University of Oulu, Finland, where he served as a Professor with the Centre for Wireless Communications. In 2006, he served as a Visiting Professor with the Ilmenau University of Technology, Ilmenau, Germany, funded by the German MERCATOR Visiting Professorship Program. Since 2007, he has been serving as a Professor with the Japan Advanced Institute of Science and Technology, Japan, while also keeping a cross-appointment position with the University of Oulu.

Prof. Matsumoto is a member of IEICE. He was a recipient of the IEEE VTS Outstanding Service Award, in 2001, the Nokia Foundation Visiting Fellow Scholarship Award, in 2002, the IEEE Japan Council Award for Distinguished Service to the Society, in 2006, the IEEE Vehicular Technology Society James R. Evans Avant Garde Award, in 2006, the Thuringen State Research Award for Advanced Applied Science, in 2006, the 2007 Best Paper Award of Institute of Electrical, Communication, and Information Engineers of Japan, in 2008, the Telecom System Technology Award by the Telecommunications Advancement Foundation, in 2009, the IEEE COMMUNICATION LETTERS Exemplary Reviewer, in 2011, the Nikkei Wireless Japan Award, in 2013, the IEEE VTS Recognition for Outstanding Distinguished Lecturer, in 2016, and the IEEE TRANSACTIONS ON COMMUNICATIONS Exemplary Reviewer, in 2018. He has led a lot of projects funded by Academy-of-Finland, European FP7, and the Japan Society for the Promotion of Science and by Japanese private companies. He has been appointed as a Finland Distinguished Professor from 2008 to 2012, funded by the Finnish National Technology Agency (Tekes) and Finnish Academy, under which he preserves the rights to participate in and apply to European and Finnish national projects. He has been serving as an IEEE Vehicular Technology Distinguished Speaker, since 2016.